Theor Chem Acc (2011) 129:677–684
DOI 10.1007/s00214-011-0930-z

REGULAR ARTICLE

Simulations of ^{129}Xe NMR chemical shift of atomic xenon dissolved in liquid benzene

Stanislav Standara · Petr Kulhánek · Radek Marek · Jan Horníček · Petr Bouř · Michal Straka

Received: 29 December 2010 / Accepted: 17 March 2011 / Published online: 1 April 2011

Abstract The isotropic ^{129}Xe NMR chemical shift of atomic Xe dissolved in liquid benzene was simulated by combining classical molecular dynamics and quantum chemical calculations of ^{129}Xe nuclear magnetic shielding. Snapshots from the molecular dynamics trajectory of xenon atom in a periodic box of benzene molecules were used for the quantum chemical calculations of isotropic ^{129}Xe chemical shift using nonrelativistic density functional theory as well as relativistic Breit–Pauli perturbation corrections. Thus, the correlation and relativistic effects as well as the temperature and dynamics effects could be included in the calculations. Theoretical results are in a very good agreement with the experimental data. The most of the experimentally observed isotropic ^{129}Xe shift was recovered in the nonrelativistic dynamical region, while the relativistic effects explain of about 8% of the total ^{129}Xe chemical shift.

Dedicated to Professor Pekka Pyykkö on the occasion of his 70th birthday and published as part of the Pyykkö Festschrift Issue.

Electronic supplementary material The online version of this article (doi:10.1007/s00214-011-0930-z) contains supplementary material, which is available to authorized users.

S. Standara · P. Kulhánek · R. Marek
National Center for Biomolecular Research, Masaryk University, Kamenice 5/A4, 62500 Brno, Czech Republic

S. Standara · J. Horníček · P. Bouř · M. Straka (✉)
Institute of Organic Chemistry and Biochemistry, Academy of Sciences of the Czech Republic, Flemingovo nám. 2, 16610 Prague, Czech Republic
e-mail: straka@uochb.cas.cz

Keywords ^{129}Xe NMR chemical shift · Dynamical averaging · Density functional theory · Breit–Pauli perturbation theory · Relativistic effects

1 Introduction

^{129}Xe atom is an excellent NMR probe. Due to its large and polarisable electron cloud the physicochemical surroundings of the ^{129}Xe atom are sensitively reflected in the magnetic shielding at its nucleus. This is expressed in the large chemical shift range of ^{129}Xe that spans several thousands of ppm in chemical compounds and several hundreds of ppm in materials containing Xe atom guest [1, 2]. The size and chemical inertness allow xenon to enter different materials without reacting chemically. The surroundings of the absorbed gas are then reflected in the NMR parameters of the ^{129}Xe nucleus, such as the chemical shift, nuclear shielding anisotropy, or NMR relaxation rates. The sensitivity of ^{129}Xe NMR spectroscopy can be increased by several orders of magnitude using hyperpolarized xenon gas [3, 4].

The ^{129}Xe NMR spectroscopy thus provides a unique tool for studying different materials and their properties. This includes studies of orientational and translational order in liquid crystals [5, 6], solvent dynamics in liquids [7], structure of porous solids [8, 9], polymers [10, 11], and clathrates [12, 13]. Glasses [14], metallo-organic frameworks [15, 16], and crystals [17] were investigated by means of ^{129}Xe NMR. Magnetic resonance imaging (MRI) based on ^{129}Xe NMR has been employed in studies of biological materials. ^{129}Xe MRI experiments use biosensors in which the ^{129}Xe atom is confined in a molecular cage, e.g., a cryptophane [18–21].

Accumulated experience exists in theoretical calculations of ^{129}Xe NMR properties of Xe molecules [22–25]

and ^{129}Xe atom guest–host systems [25–36]. State-of-the-art calculations of NMR parameters in Xe dimer and in Xe gas have been reported by Hanni et al. [37–39].

This work was motivated by the recent computational study on ^{129}Xe chemical shift in Xe@C_{60}, in which we observed a large discrepancy between the theoretical (152.9 ppm) [40] and experimental (179.2 ppm) [41] isotropic chemical shifts. The theoretical value was obtained at well-calibrated density functional (DFT) BHandHLYP level, which mimicked accurate CCSD(T) results for the Xe…benzene model system. The results included correlated relativistic Breit–Pauli perturbation theory (BPPT) contributions ($\sim$10%), corrections for intramolecular dynamics ($\sim$10%), and implicit solvent effects (<0.1%) [40]. The remaining large discrepancy between the theoretical and the experimental results opened a question about the role of the dynamical solvent–solute effects, which have not been included in calculations. Therefore, in the current study, we build a dynamical model of xenon dissolved in benzene, as an initial step to the more complicated Xe@C_{60} problem. To our best knowledge, even the problem of ^{129}Xe chemical shift in benzene has not been tackled theoretically yet.

Experimental measurements on ^{129}Xe dissolved in liquids show ^{129}Xe chemical shift between 85 ppm (in C_6F_6) and 247 ppm (in CH_2I_2) [1, 41–43]. For benzene solvent, Syamala et al. reported the value of 188.14 ppm [41], Stengle et al. reported 193.0 ppm [42], and Miller et al. measured 195 ppm [43].

Theoretical studies by Jameson et al. used so-called chemical shift function in combination with Monte-Carlo (MC) molecular dynamics (MD) methods to simulate the xenon shift in liquids [33], clathrates [34, 35], and cryptophane cages [36]. The chemical shift function describes the shielding response of the ^{129}Xe atom at different spatial configurations of the studied system. It can be parameterized by quantum chemical calculations on either experimentally known systems, such as clathrates [34, 35], or on model Xe systems, such as Xe–CH_4 and Xe–CO_2 dimers [44]. The averaged ^{129}Xe shift is evaluated from the configurations of the system sampled by Monte-Carlo methods using the chemical shift function [33].

A somewhat different approach is applied in the present work. We calculate the chemical shift quantum chemically (QC) from snapshots of a classical MD trajectory of a system with Xe atom dissolved in a periodic box of benzene molecules. The main reason for using this method is that for larger Xe systems it is very difficult to precisely parameterize the chemical shift function. Additionally, each snapshot can be evaluated quantum mechanically, and thus, the tiny details of the electronic response of Xe atom to the environment are obtained directly from quantum chemical calculations without any parameterization. This also presents a certain limitation as the QC calculations are demanding, and hence, the calculated snapshots are limited in size. However, the size limitation should introduce only marginal errors because of the local nature of the nuclear magnetic shielding. It can be well controlled by looking at the influence of the cluster size on the calculated values. Methods using snapshots from MD simulations to calculate dynamically averaged molecular properties have been successfully used in numerous studies of molecular properties. For examples, see refs. [45–50].

The QC methods used in the present study were calibrated in our recent work on Xe@C_{60} [40]. Special emphasis is given to accounting for the relativistic effects, which are important in the ^{129}Xe NMR calculations. The importance of relativistic effects in heavy elements has been well documented in the famous reviews on relativistic effects by Pyykkö [51, 52]. In the present work, the relativistic corrections to ^{129}Xe nuclear shielding are evaluated using the Breit–Pauli perturbation theory [53–55].

In the following, we discuss the computational details (Sect. 2), simulations of liquid benzene and Xe in liquid benzene (Sects. 3.1 and 3.2), preparation and nonrelativistic calculations of snapshots from MD (Sect. 3.3) as well as relativistic BPPT calculations of snapshots (Sect. 3.4). The conclusions are summarized in Sect. 4.

2 Computational details

2.1 Molecular dynamics simulations

All MD simulations were carried out using the AMBER 10 software [56]. Two cubic boxes, one with 1,331 molecules of benzene and other with 1,330 molecules of benzene as well as a Xe atom were built and minimized using the periodic boundary conditions. The non-bonded cutoff value of 11.0 Å was used. The electrostatic interaction beyond this cutoff limit was treated by the Particle Mesh Ewald (PME) summation method [57], whereas far Lennard–Jones (LJ) interactions were neglected. We have tested two force field models (Table 1): (a) The general amber force field (GAFF) [58] as implemented in AMBER with RESP [59] charges calculated at the HF level (model A), and (b) the model with modified Lennard–Jones potential parameters from ref. [60] (model B in Table 1). Xenon LJ parameters were taken from literature [61], see Table 1.

In the first equilibration step, the system was heated for 200 ps from 1 to 300 K within the NVT condition applying the Langevin stochastic thermostat, with a collision frequency $\gamma = 5.0$ ps^{-1}. The next step was 500 ps of MD simulation in the isobaric–isothermal NPT ensemble at 1 atm and 300 K. The pressure relaxation time was set to $t_P = 1.2$ ps, collision frequency to $\gamma = 2.0$ ps^{-1}, and the

Table 1 Van Der Waals radius (r/Å) and the 6–12 potential well-depth parameters (ε/kcal mol^{-1}) of force fields A and B

Atom	Model A		Model B	
	r/Å	ε/kcal mol^{-1}	r/Å	ε/kcal mol^{-1}
C	1.9080	0.086	1.9924	0.070
H	1.4590	0.015	1.3582	0.030
Xe	2.2309	0.4264	2.2309	0.4264
	Atomic charge		Atomic charge	
C	−0.130		−0.115	
H	0.130		0.115	

nonbonded cutoff value to 15.0 Å. Bonds involving hydrogens were constrained using the SHAKE algorithm [62]. All simulations were done using integration time step of 1 fs. The final size of the box edge after equilibration was 58.6 Å. The production run was taken for 1 ns at NPT conditions. Coordinates were stored each 0.5 ps. For refining the angular radial distribution functions, additional 5 ns NPT dynamics was performed.

2.2 Nonrelativistic NMR chemical shifts

The DFT calculations of the snapshots were limited to the first solvation shell, see Sect. 3.2. Nuclear shielding calculations were carried out at the DFT-GIAO (Gauge-Including Atomic Orbitals) [63] level of theory as implemented in the Gaussian 09 (ref. [64]) software. The exchange-correlation BHandHLYP functional [65, 66] in a combination with the [22s17p14d2f/15s13p11d2f] basis set for Xe referred to as MHA (ref. [40]) was employed. The SVP [67] basis set was used for C and H atoms. Initial tests have shown that the basis set superposition error (BSSE) corrections are small, below 1 ppm. Therefore, no BSSE corrections were added in the production work.

For testing purposes, the implicit solvent was simulated by the polarizable continuum model (PCM) [68, 69], employing the IEF–PCM model implemented in Gaussian 09 [64].

In a typical ^{129}Xe NMR experiment, Xe gas at one atmosphere is used as a reference. For practical reasons, we used the nuclear shielding of ^{129}Xe atom *in vacuo* as reference. This introduces a small error within 0.5 ppm in the computational data, corresponding to the Xe gas versus Xe atom chemical shift [33]. The calculated isotropic shielding constants were converted into chemical shifts in the usual manner:

$$\delta_{\mathrm{Xe}} \approx \left[\sigma_{\mathrm{st(Xe\,atom)}} - \sigma_{i\mathrm{(Xe\,in\,benzene)}}\right] / \left[1 - \sigma_{\mathrm{st(Xe\,atom)}}\right], \quad (1)$$

where σ_{st} and σ_i are the shielding constants (in ppm) of the reference xenon atom *in vacuo* and of the xenon atom in benzene calculated at the same level of theory.

To verify the time correlation of the data and to estimate the standard deviation of the average of the ^{129}Xe shift, the block-averaging method was used [70–72]. In this procedure, the calculated dataset is systematically divided into blocks of increasing size, and individual averages are calculated for each block until the size of a block is large enough so that the data in the neighboring blocks become uncorrelated. At this point, the standard deviation of the average, s_x, reaches a plateau. We used a coarsed-grained blocking method in which typically more values inside a thought uncorrelated block are utilized in the calculations.

2.3 Relativistic Breit–Pauli perturbation theory corrections to NMR chemical shift

Details of BPPT can be found elsewhere [53–55]. A total of 16 relativistic contributions to the nuclear shielding are obtained in the one-electron leading-order BPPT. Of these, only five shielding contributions are important in the calculations of relative chemical shift [22, 23, 37, 40]. These are the second-order singlet $\sigma^{\mathrm{p\text{-}KE/OZ}}$, the third-order singlet $\sigma^{\mathrm{p/mv}}$ and $\sigma^{\mathrm{p/Dar}}$ as well as the third-order triplet $\sigma^{\mathrm{FC\text{-}I}}$ and $\sigma^{\mathrm{SD\text{-}I}}$ terms. The $\sigma^{\mathrm{p/mv}}$, $\sigma^{\mathrm{p/Dar}}$, and $\sigma^{\mathrm{p\text{-}KE/OZ}}$ were calculated in the production work, as the $\sigma^{\mathrm{FC\text{-}I}}$ and $\sigma^{\mathrm{SD\text{-}I}}$ terms were found small in the present system, see Sect. 3.4 for details.

An in-house version of the Dalton 2.0 [73] code was employed for the BPPT calculations. BPPT corrections were calculated using a common gauge origin (CGO) placed at the Xe atom. The more reliable GIAO approach is not implemented within the BPPT framework. We note, however, that while usage of CGO can cause severe inaccuracies in the nonrelativistic nuclear shielding calculations, it works well in the BPPT framework, provided that the common gauge origin is placed at atom with the largest electron density. This was shown in previous studies, see, e.g., [23].

Uncontracted FIVu61 basis set [27s23p22d2f] developed by Lantto [22, 23, 40] was used for Xe, and the SVP basis set was used for C and H. The initial guess in the SCF step was pre-calculated using the Turbomole 6.0 package [74]. Xe atom *in vacuo* was used as a reference, see Eq. 1.

3 Results and discussion

3.1 Simulations of pure liquid benzene

To build the model systematically, we started with simulations of pure benzene. The general amber force field (GAFF) implemented in Amber somehow underestimates the density of the benzene (0.857 g/cm^3) when compared to the experimental one (0.874 g/cm^3) [75] at 298 K.

Hence, we adopted more recent force field parameters for C and H atoms [60], which marginally improved the density to 0.861 g/cm^3 at 300 K. The modified force field (model B in Table 1) was used in the production work.

Figure 1 shows the radial distribution function (RDF) for the centers of mass of benzene molecules. The first maximum on RDF corresponding to the first coordination shell at 5.6 Å is in agreement with previous computational studies of benzene dynamics [60, 76]. The integrated RDF peak provides a coordination number of 13, which is close to the value of 12 suggested in previous works [60, 76]. For detailed studies of different aspects of the dynamics and microscopic structure of liquid benzene, we refer the reader to refs. [60, 76]. We now proceed to the Xe–benzene system.

3.2 Simulations of atomic Xe in liquid benzene

The benzene–benzene radial distribution function in the Xe–benzene system is basically identical to that of pure benzene; the two curves coincide in Fig. 1. The RDF for the distance of the benzene center of mass from the Xe atom has first maximum at $R = 5.3$ Å, Fig. 1. Thus, the cavity around the Xe atom is smaller than that surrounding a benzene molecule. The integral value under the first peak in Xe–benzene RDF in Fig. 1 gives a coordination number of 10, smaller than that for the benzene itself (13, vide supra). Radial distribution functions for pairs of atoms in Xe–benzene system are given in supporting information, Figs. S1 and S2.

To obtain more detailed information on the microscopic structure of the Xe–benzene system, we calculated the Xe–benzene and benzene–benzene angular radial distribution functions (Figs. 2 and 3) from the 5 ns trajectory of the system. The first solvation shell around the Xe atom is well

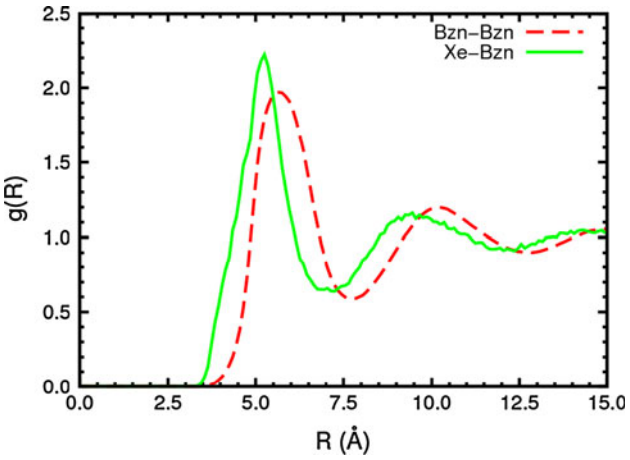

Fig. 1 Radial distribution functions for benzene–benzene (Bzn-Bzn) and xenon–benzene pairs (Xe–Bzn) using the benzene centers of mass

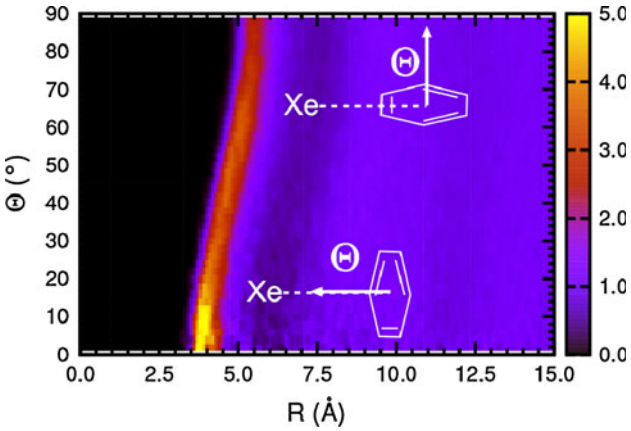

Fig. 2 Xe–benzene angular radial distribution function in the Xe–benzene system. R corresponds to distance from Xe to the center of mass of benzene. Θ is the angle between vector pointing from Xe to the center of mass of the benzene and the normal to the benzene plane (obtained as a best fit from the benzene atoms). Notice the less resolved second solvation shell

resolved and partially ordered (Fig. 2). The "T"-like configuration ($\Theta = 0°$ in Fig. 2) with Xe on the normal of the benzene plane passing through the center of the mass of benzene is more populated configuration than the one with Xe in the plane of a benzene molecule ($\Theta = 90°$). The change from $\Theta = 0°$ to $\Theta = 90°$ is rather smooth. Corresponding increase in the radial part (Xe to center of mass of benzene) is observed in Fig. 2. The less resolved second solvation shell appears to be more diffuse and more isotropic, Fig. 2. This suggests that in snapshot calculations of the ^{129}Xe nuclear magnetic shielding, the solvent effects outside the first solvation shell can be treated by implicit solvent models. However, the influence of solvent molecules beyond the first solvation shell on ^{129}Xe shift is small as shown in Sect. 3.3.

The benzene–benzene angular radial distribution function in the Xe–benzene system in Fig. 3 is very similar to that in pure benzene (not shown) [76] and shows that the most preferred configuration at short separations corresponds to a perpendicular orientation of two benzenes while the solvent appears rather isotropic in angular distribution beyond the first solvation shell.

3.3 Calculations of ^{129}Xe NMR chemical shift from MD snaphots

Calculations of full-size snapshots for Xe atom surrounded with over a thousand benzene molecules are currently far beyond the limits of quantum chemical methods. Hence, we only included the equivalent of the first solvation shell in the calculations and estimated errors induced by this approximation. We processed selected snapshots and included only benzenes which reach by any of their atoms a

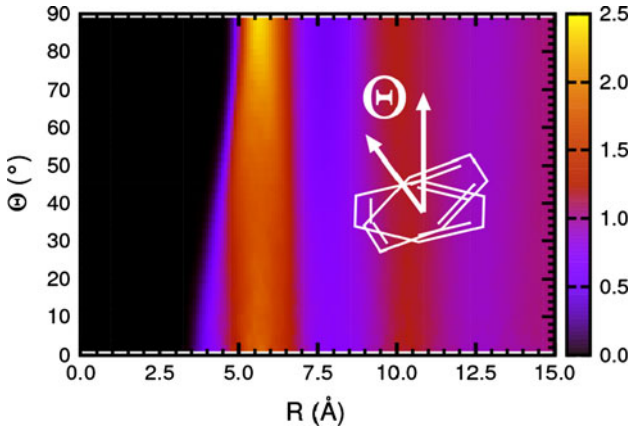

Fig. 3 Benzene–benzene angular radial distribution function in Xe–benzene system. R is distance between the centers of mass of benzenes. Θ is angle between the normals of the benzene planes

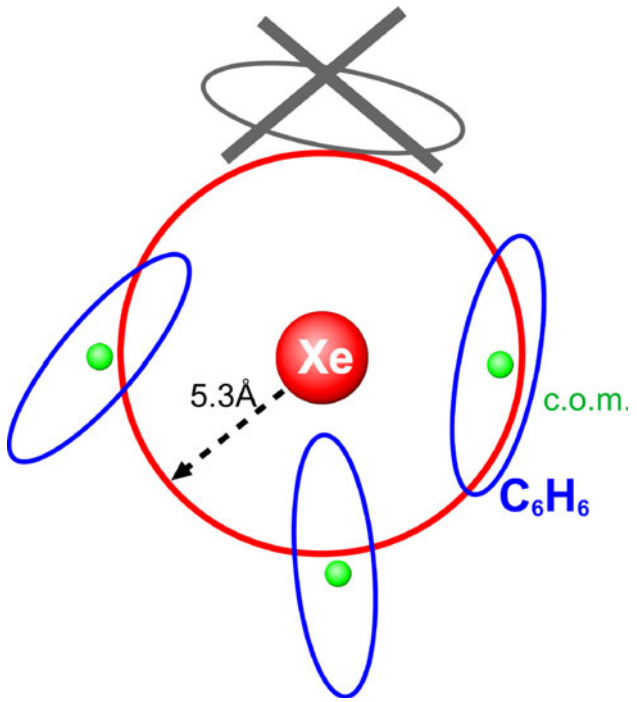

Fig. 4 Truncation of the snapshots beyond the first solvation shell for use in the quantum chemical calculations

5.3 Å sphere (maximum on radial distribution function in Fig. 1) surrounding the Xe atom. The procedure is schematically shown in Fig. 4. This led to snapshots with typically 9–10 benzenes, corresponding to the calculated coordination number 10, see above. Several snapshots with less (6–8) or more (11–13) benzenes were present in the dataset, as detailed in the distribution diagram (Fig. S3).

To test for the errors caused by omitting benzene molecules beyond the first solvation shell, we selected a few snapshots for which we included additional 3, 6, and 9 benzene molecules beyond the first solvation shell. Only changes of 1–2 ppm, smaller than the statistical error of ca 3 ppm estimated below were found, see Table 2. Hence, the first solvent shell approximation is justified. As a further check, we switched on the PCM model in the QC calculations. Marginal changes within 2 ppm were observed in the tested snapshots (Table 2). The production calculations did not use PCM due to the rather slow convergence of PCM calculations.

Note that while using the DFT may be very problematic, e.g., for energetics and structures in weakly bonded systems, for NMR parameters the situation is different. There is accumulating evidence that DFT and especially the BHandHLYP functional provides excellent results for noble gas NMR parameters in weakly bonded systems [40, 77, 78]. It was pointed out that it is not the dispersion but the exchange–overlap interaction which is crucial for the ^{129}Xe response to the magnetic field [33, 79].

Results for the time-averaged nonrelativistic ^{129}Xe chemical shift are summarized in Table 3. A total 500 snapshots of 500 ps trajectory led to the averaged ^{129}Xe shift of 176.2 ± 3.3 ppm. Including additional 500 snapshots in a total of 1,000 ps trajectory brought only marginal changes leading to the averaged value of ^{129}Xe chemical shift of 176.1 ± 2.5 ppm. This results can be considered as converged at the nonrelativistic level. Figure 5 shows the distribution of the calculated instantaneous ^{129}Xe chemical shifts, exhibiting approximately a Gaussian profile. The standard deviation of the full sample ($\sigma_x = 54.4$ ppm) in Table 3 shows how dispersed is the instantaneous ^{129}Xe shielding, while the standard deviation of the average ($s_x = 2.5$ ppm) provides an estimate of the error of the averaged shift.

The calculated nonrelativistic value of 176.1 ± 2.5 ppm is somewhat below the range of the observed experimental values of 188–195 ppm [41–43]. We proceed to the relativistic BPPT corrections.

3.4 Relativistic BPPT corrections to ^{129}Xe NMR chemical shift

The relativistic BPPT corrections to the nuclear magnetic shielding are computationally by an order of magnitude more demanding than the nonrelativistic calculations. For this reason, we had to limit the number of the snapshots for BPPT. Furthermore, we noticed that of the five dominant BPPT contributions, the two computationally most demanding third-order triplet terms, $\sigma^{\text{FC-I}}$ and $\sigma^{\text{SD-I}}$, are by an order of magnitude smaller than the remaining three dominant contributions, $\sigma^{\text{p/mv}}$, $\sigma^{\text{p/Dar}}$, and $\sigma^{\text{p-KE/OZ}}$ (Table S4). This trend was incidentally observed for Xe@C_{60} in ref. [40], but remained unnoticed in there. Hence, we calculated only the $\sigma^{\text{p/mv}}$, $\sigma^{\text{p/Dar}}$, and $\sigma^{\text{p-KE/OZ}}$ BPPT terms in the series of truncated snapshots. This approximation is referred to as BPPT-3 in the following discussion.

Table 2 The accuracy of the 1st solvent shell approximation

Snapshot	1st shell	1st shell + 3Bzn	1st shell + 6Bzn	1st shell + 9Bzn	1st shell + PCM
256	149.6	149.6	151.0	151.1	149.4
508	133.0	133.5	133.2	133.8	132.9
1,024	169.5	169.8	171.8	171.8	169.3

Calculated nonrelativistic ^{129}Xe chemical shift (in ppm) for selected snapshots truncated to the first solvation shell with either additional 3–9 benzene molecules or in PCM model

Table 3 Summary of statistical averaging of calculated truncated snapshots

Method	No. of snapshots	Trajectory (ps)	^{129}Xe shift (ppm)	σ_x (ppm)	s_x (ppm)
NR[a]	500	0–500	176.2	55.8	3.3
NR[a]	500	500–1,000	175.9	53.7	3.7
NR[a]	1,000	1,000	176.1	54.4	2.5
BPPT[b]	125	500	15.3	4.6	0.4
NR[a] + BPPT[b]	1,000,125	1,000,500	191.4	54.6	2.5
Exp.			188.14[c], 193.0[d], 195[e]		

[a] Nonrelativistic BHandHLYP/MHA/SVP

[b] Relativistic BHandHLYP/FIVu61/SVP

[c] Ref. [41]

[d] Ref. [42]

[e] Ref. [43]

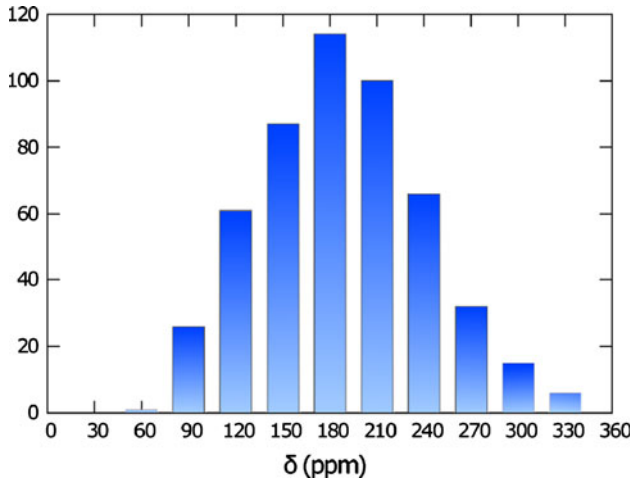

Fig. 5 Distribution of the calculated nonrelativistic ^{129}Xe shifts using 512 snapshots of the 512 ps trajectory

Different BPPT terms ($\sigma^{p/mv}$, $\sigma^{FC\text{-}SZ/KE}$, $\sigma^{FC\text{-}II}$) than those mentioned above were found to be dominant in ^{113}Cd chemical shift calculations of system with Cd^{II} ion dissolved in aqueous solution [44]. This is due to different types of electronic structures and underlying interactions in these two systems. In our case, we have Xe atom with $6p^6$ valence shell weakly interacting with surrounding benzene molecules while strong donor–acceptor bonds are formed in Cd^{II}-water system in which Cd^{II} with $4d^{10}$ valence shell forms stable $[Cd^{II}(H_2O)_6]^{2+}$ donor–acceptor complex [44].

A set of 125 snapshots of the initial 500 ps trajectory gave BPPT-3 relativistic correction to ^{129}Xe shift of $+15.3 \pm 0.4$ ppm. This result is on a scale expected on the basis of the previous theoretical studies of NMR parameters in weakly bonded Xe compounds [37, 40].

Adding now the BPPT-3 correction of 15.3 ± 0.4 ppm to the nonrelativistic NMR chemical shift of 176.1 ± 2.5 ppm, we arrive at the final value of 191.4 ± 2.5 ppm for the isotropic chemical shift of ^{129}Xe atom dissolved in liquid benzene at 300 K and 1 atm. The computational result is in an excellent agreement with the experimental data ranging from 188.14 to 195 ppm (Table 3). While we have no doubts that this excellent result is partly gaining from the different error cancellations, the present model seems to work very well. Errors due to the several approximations should lie within the margins of the statistical errors given above. They come from the deficiencies of MD force field, neglecting the benzenes beyond the first solvation shell (<2 ppm), DFT approximation, basis set size effects (<1 ppm), and neglecting the smaller BPPT terms (<1 ppm). In spite of these uncertainties, we feel that our work clearly shows the advantages of the multi-scale MD/QC computations of the xenon shift in liquids. The procedure is not dependent on special empirical parameters and also provides insight into the physical circumstances influencing the shift, including the time-fluctuations and dynamical dispersion.

4 Conclusions

A box of benzene molecules surrounding xenon atom was subjected to the classical molecular dynamics run. Snapshots from the trajectory were reduced to the first solvation shell and used in the quantum chemical calculations of the ^{129}Xe chemical shift, both at the nonrelativistic and relativistic BPPT levels. The resulting time-averaged isotropic ^{129}Xe chemical shift was calculated to be 191.4 ± 2.5 ppm, which is in excellent agreement with the previously reported experimental data, ranging between 188 and 195 ppm. The relativistic corrections were found to be dominated by the three leading-order BPPT terms ($\sigma^{\text{p-KE/OZ}}$, $\sigma^{\text{p/mv}}$ and $\sigma^{\text{p/Dar}}$) and represent about 8% of the total calculated chemical shift.

Based on these results, we believe that the present approach can be extended to the practical simulations of the ^{129}Xe chemical shift in isotropic liquids. The calculations for more complex xenon guest–host systems should also be feasible, provided that reliable force field is available and that the interactions of ^{129}Xe with the surroundings are local enough so that the size of the snapshots is not prohibitive for the quantum chemical calculations.

Acknowledgments We thank to Perttu Lantto and Juha Vaara for valuable discussions and providing the BPPT version of the Dalton code. The project was supported by the Academy of Sciences of the Czech Republic Z04 055 905 (MS, JH, PB) and M200550902 (PB), Czech Science Foundation (Grants No. 203/09/2037, P208/11/0105), Ministry of Education of the Czech Republic (MSM0021622413 to SS, PK, RM), European Reintegration Grant No. 230955 (MS), and the Grant No. 205872 (PK) within the 7th European Community Framework Program. Computational resources were partially provided by the Metacentrum, Czech Republic (MSM6383917201). Jan Lazebníček is acknowledged for initial testing calculations.

References

1. Gerken M, Schröbilgen G (2000) Coord Chem Rev 197:335
2. Ratcliffe CI (1998) Annu Rep NMR Spectrosc 36:123
3. Happer W, Miron E, Schaefer S, Schreiber D, van Wijngaarden WA, Zeng Z (1984) Phys Rev A 29:3092
4. Goodson BM (2002) J Magn Reson 155:157
5. Jokisaari J (2003) In: Burnell EE, de Lange CA (eds) NMR of ordered liquids. Kluwer, Dordrecht, pp 109–135
6. Jokisaari J (2009) In: Dong R (ed) Nuclear magnetic resonance spectroscopy of liquid crystals. World Scientific Publishing Co Pte Ltd, Singapore, pp 79–116
7. Jokisaari J (1994) Prog Nucl Magn Reson Spectrosc 26:1
8. Raftery D, Chmelka BF (1994) NMR Basic Princ Prog 30:111
9. Romanenko KV (2010) Ann Rep NMR Spect 69:1
10. Yampolskii YP (2007) Russ Chem Rev 76:59
11. Nagasaka B, Omi H, Eguchi T, Nakayama H, Nakamura N (2001) Chem Phys Lett 340:473
12. Yang L, Tulk C, Klug D, Moudrakovski I, Ratcliffe C, Ripmeester J, Chakoumakos B, Ehm L, Martin D, Parise J (2009) Proc Nat Acad Sci 106:6060
13. Ripmeester JA, Tse JS, Ratcliffe CI, Powell BM (1987) Nature 325:135
14. Moudrakovski I, Sanchez A, Ratcliffe CI, Ripmeester J (2004) J Phys Chem B 104:7306
15. Springuel-Huet M-A, Nossov A, Adem A, Guenneau F, Volkringer C, Loiseau T, Ferey G, Gedeon A (2010) J Am Chem Soc 132:11599
16. Ooms KJ, Wasylishen RE (2007) Microp Mesop Mat 103:341
17. Comotti A, Bracco S, Sozzani P, Horike S, Matsuda R (2007) Chem Comm 2007:350
18. Taratul O, Dmochowski IJ (2010) Curr Opin Chem Bio 14:97
19. Berthault P, Huber G, Desvaux H (2009) Prog Nuc Mag Res Spect 55:35
20. Chambers MJ, Hill PA, Aaron JA, Han Z, Christianson DW, Kuzma NN, Dmochowski IJ (2009) J Am Chem Soc 131:563
21. Schlundt A, Kilian W, Beyermann M, Sticht M, Günther S, Höpner S, Falk K, Roetzschke O, Mitschang L, Freund C (2009) Angew Chem Int Ed 48:4142
22. Straka M, Lantto P, Räsänen M, Vaara J (2007) J Chem Phys 127:234314
23. Lantto P, Vaara J (2007) J Chem Phys 127:084312
24. Cukras J, Sadlej J (2008) Chem Phys Lett 467:18
25. Bagno A, Saielli G (2003) Chem Eur J 9:1486
26. Kantola JH, Vaara J, Rantala T, Jokisaari J (1997) J Chem Phys 107:6470
27. Autschbach J, Zurek E (2003) J Phys Chem A 107:4967
28. Bühl M, Patchkovskii S, Thiel W (1997) Chem Phys Lett 275:14
29. Sears DN, Jameson CJ (2003) J Chem Phys 118:9987
30. Lintuvuori J, Straka M, Vaara J (2007) Phys Rev E 75:31707
31. Jameson CJ, Sears DN, de Dios AC (2003) J Chem Phys 118:2575
32. Sears DN, Wasylishen RE, Ueda T (2006) J Phys Chem B 110:11120
33. Jameson CJ, Sears DN, Murad S (2004) J Chem Phys 121:9581
34. Jameson CJ, Stueber D (2004) J Chem Phys 120:10200
35. Stueber D, Jameson CJ (2004) J Chem Phys 120:1560
36. Sears DN, Jameson CJ (2003) J Chem Phys 119:12231
37. Hanni M, Lantto P, Iliaš M, Jensen HJAa, Vaara J (2007) J Chem Phys 127:164313
38. Hanni M, Lantto P, Runeberg N, Jokisaari J, Vaara J (2004) J Chem Phys 121:5908
39. Hanni M, Lantto P, Vaara J (2009) Phys Chem Chem Phys 11:2485
40. Straka M, Lantto P, Vaara J (2008) J Phys Chem A 112:2658
41. Syamala MS, Cross RJ, Saunders M (2002) J Am Chem Soc 124:6216
42. Stengle TR, Reo NV, Williamson KL (1981) J Phys Chem 85:3772
43. Miller KW, Reo NV, Uiterkamp AJMS, Stengle DP, Stengle TR, Williamson KL (1981) Proc Natl Acad Sci USA 78:4946
44. Sears DN, Jameson CJ (2004) J Chem Phys 121:2151
45. Malkin VG, Malkina OL, Steinebrunner G, Huber H (2006) Chem Eur J 2:452
46. Asher JR, Doltsinis NL, Kaupp M (2004) J Am Chem Soc 126:9854
47. Pennanen TS, Vaara J, Lantto P, Sillanpää AJ, Laasonen K, Jokisaari J (2004) Am Chem Soc 126:11093
48. Bühl M, Grigoleit S, Kabrede H, Mauschick FT (2005) Chem Eur J 12:477
49. Li X, Rinkevicius Z, Yaoquan T, Tian H, Agern H (2008) J Phys Chem B 112:11347–11352
50. Dračínský M, Kaminský J, Bouř P (2009) J Phys Chem B 113:14698
51. Pyykkö P (1978) Adv Quant Chem 11:353
52. Pyykkö P (1988) Chem Rev 88:563

53. Vaara J, Manninen P, Lantto P (2004) In: Kaupp M, Bühl M, Malkin VG (eds) Calculations of NMR and EPR parameters: theory and applications. Wiley-VCH, Weinheim, pp 209–226
54. Manninen P, Lantto P, Vaara J, Ruud K (2003) J Chem Phys 119:2623
55. Manninen P, Ruud K, Lantto P, Vaara J (2005) J Chem Phys 122:114107, Erratum: J Chem Phys (2006) 124:149901
56. Case DA, Darden TA, Cheatham III TE, Simmerling CL, Wang J, Duke RE, Luo R, Crowley M, Walker RC, Zhang W, Merz KM, Wang B, Hayik S, Roitberg A, Seabra G, Kolossváry I, Wong KF, Paesani F, Vanicek J, Wu X, Brozell SR, Steinbrecher T, Gohlke H, Yang L, Tan C, Mongan J, Hornak V, Cui G, Mathews DH, Seetin MG, Sagui C, Babin V, Kollman PA (2008) AMBER 10, University of California, San Francisco
57. Darden T, York D, Pedersen L (1993) J Chem Phys 98:10089
58. Wang JM, Wolf RM, Caldwell JW, Kollman PA, Case DA (2004) J Comput Chem 25:1157
59. Bayly CI, Cieplak P, Cornell WD, Kollman PA (1993) J Phys Chem B 97:10269
60. Chelli R, Cardini G, Ricci M, Bartolini P, Righini R, Califano S (2001) Phys Chem Chem Phys 3:2803 and references therein
61. Paschek D (2004) J Chem Phys 120:6674
62. Ryckaert JP, Ciccotti G, Berendsen HJC (1977) J Comput Phys 23:327
63. Wolinski K, Hinton JF, Pulay P (1990) J Am Chem Soc 112:8251
64. Frisch MJ, Trucks GW, Schlegel HB, Scuseria GE, Robb MA, Cheeseman JR, Scalmani G, Barone V, Mennucci B, Petersson GA, Nakatsuji H, Caricato M, Li X, Hratchian HP, Izmaylov AF, Bloino J, Zheng G, Sonnenberg JL, Hada M, Ehara M, Toyota K, Fukuda R, Hasegawa J, Ishida M, Nakajima T, Honda Y, Kitao O, Nakai H, Vreven T, Montgomery JA Jr, Peralta JE, Ogliaro F, Bearpark M, Heyd JJ, Brothers E, Kudin KN, Staroverov VN, Kobayashi R, Normand J, Raghavachari K, Rendell A, Burant JC, Iyengar SS, Tomasi J, Cossi M, Rega N, Millam JM, Klene M, Knox JE, Cross JB, Bakken V, Adamo C, Jaramillo J, Gomperts R, Stratmann RE, Yazyev O, Austin AJ, Cammi R, Pomelli C, Ochterski JW, Martin RL, Morokuma K, Zakrzewski VG, Voth GA, Salvador P, Dannenberg JJ, Dapprich S, Daniels AD, Farkas O, Foresman JB, Ortiz JV, Cioslowski J, Fox DJ (2009) GAUSSIAN 09, Revision A.02. Gaussian, Inc., Wallingford
65. Becke AD (1993) J Chem Phys 98:5648
66. Becke AD (1988) Phys Rev A 38:3098
67. Schäfer A, Horn H, Ahlrichs R (1992) J Chem Phys 97:2571
68. Miertuš S, Scrocco E, Tomasi J (1981) Chem Phys 55:117
69. Tomasi J, Mennucci B, Cammi R (2005) Chem Rev 105:2999
70. Flyvbjerg H, Petersen HG (1989) J Chem Phys 91:461
71. Jensen F (2007) Introduction to computational chemistry, second edition. Willey-VCH, Weinheim, pp 468–772
72. Leach AR (2001) In: Molecular modelling principles and applications, second edition. Pearson Prentice Hall, Edinburgh, pp 343–347
73. DALTON (2005) A molecular electronic structure program, release 2.0. See http://www.kjemi.uio.no/software/dalton/dalton.html for the latest version
74. Ahlrichs R, Bär M, Häser M, Horn H, Kölmel C (1989) Electronic structure calculations on workstation computers: the program system TURBOMOLE. Chem Phys Lett 162:165
75. CRC (2006-2007) In: DD Lide (ed) Handbook of chemistry and physics. Taylor and Francis, Boca Raton
76. Headen TF, Howard CA, Skipper NT, Wilkinson MA, Bowron DT, Soper AK (2010) J Am Chem Soc 132:5735 and references therein
77. Straka M, Vaara J (2006) J Phys Chem A 110:12338
78. Štěpánek P, Bouř P, Straka M (2010) Chem Phys Lett 500:54
79. Adrian FJ (2004) J Chem Phys 120:8469